Roughness-induced mechanisms for electron scattering in wurtzite group-III-nitride heterostructures

Doan Nhat Quang
Center for Theoretical Physics, Vietnamese Academy of Science and Technology, P.O. Box 429, Boho, Hanoi 10000, Vietnam

Vu Ngoc Tuoc, Nguyen Huyen Tung, Nguyen Viet Minh, and Pham Nam Phong
Institute of Engineering Physics, Hanoi University of Technology, 1 Dai Co Viet Road, Hanoi, Vietnam
(Received 13 July 2005; revised manuscript received 14 October 2005; published 2 December 2005)

We present a theory of the low-temperature mobility of the two-dimensional electron gas (2DEG) in wurtzite group-III-nitride heterostructures, e.g., AlGaN/GaN, taking adequate account of the roughness-induced scattering mechanisms and the effect due to sheet polarization charges. The squeeze of the electron distribution in the quantum well by positive piezoelectric and spontaneous polarization-induced charges on the interface is calculated in an analytic form. Thus, we obtained simple expressions describing the squeeze-related enhancement of the 2DEG screening and the unscreened potentials for different scattering sources. Altogether, their screened potentials may be strongly enhanced, so that the 2DEG mobility may be remarkably reduced by sheet polarization charges. Moreover, we proved that the roughness-induced piezoelectric charges and the roughness-induced deformation potential exhibit new important scattering mechanisms governing the 2DEG transport in wurtzite III-nitride heterostructures. The partial 2DEG mobilities limited by them may be of the order of or less than 10^3 cm^2/V s. Our theory turns out to be successful in the quantitative explanation of recent experimental data about the high-density 2DEG mobility, e.g., its nonmonotonic dependence on carrier density and its enhancement in the double heterostructure, which have not been understood starting merely from the conventional scattering mechanisms.

DOI: 10.1103/PhysRevB.72.245303 PACS number(s): 73.50.Bk, 73.63.Hs, 77.65.Ly

I. INTRODUCTION

Group-III-nitride-based heterostructures, in particular, the AlGaN/GaN high electron mobility transistor, have been a subject of many recent intense investigations because of their promising potential for high-voltage, high-power, and high-temperature microwave applications.[1–6] The electron mobility is an important transport parameter used to characterize the performance of high electron mobility transistor structures. Various studies have reported on electrical conductivity of the two-dimensional electron gas (2DEG) in AlGaN/GaN samples. In the majority of cases, these studies have been focused on the experimental observation[7–13] and theoretical explanation[14–18] of the dependence of the electrical conductivity on temperature and Al content.

However, for device applications one is also interested in the variation of the 2DEG mobility with sheet carrier density. The experimental observation at high electron densities ($\gtrsim 5\times 10^{12}$ cm^{-2}) revealed the following striking features. First, this variation exhibits a nonmonotonic function with a pronounced maximum. In one case,[9,19–21] the measured result was reported with no theoretical analysis. In another case,[12] the theory had to invoke the concept of interface charges of an extremely high areal density (up to 2×10^{13} cm^{-2}), but with no clarification of their nature. They might be interface ionized impurities. However, this concept was shown[22,23] to be very suspect even at a much lower density of interface impurity charges ($\sim 10^{11}$ cm^{-2}). Second, in comparison to an AlGaN/GaN single heterostructure (SH), the mobility in the respective AlGaN/GaN/AlGaN double heterostructure (DH) is significantly enhanced, its peak being raised and shifted toward lower electron densities.[19]

To date, the abovementioned experimental findings have not been satisfactorily interpreted, so remaining as challenging problems in the transport theory of III-nitride heterostructures. It was believed[24] that the existing set of so far-known scattering mechanisms is insufficient for 2DEGs in these systems.

It is well known that in heterostructures made from III-nitrides and their alloys, there exist strong polarization effects in the [0001] orientation, viz., piezoelectric[25] and spontaneous[26] polarizations. These induce a uniform density of positive sheet polarization charges bound on the interface. The charges may give rise to remarkable modifications in the potential profile.[18,19,27–29] In particular, they squeeze the 2DEG, so pushing them closer to the interface. Hereafter, this squeeze of the electron distribution is referred to as a polarization confinement effect. This may lead to significant changes in the observable properties of the 2DEG, e.g., its mobility.

It is worth mentioning that the disorder in a system may strongly influence its polarizability. The effects due to alloy disorder and interface roughness on the 2DEG mobility are then twofold. On one hand, the disorders act themselves as a short-range scattering source. On the other hand, they act as an essential factor for the creation of a new (long- or short-range) scattering source. Recently, Jena and co-workers[24] have shown that in AlGaN/GaN heterostructures alloy disorder causes random nonuniform fluctuations in magnitude of the microscopic dipoles distributed at Ga and Al sites in the barrier. The 2DEG mobility limited by alloy disorder-related dipole scattering is equal to or greater than 2×10^5 cm^2/V s.

Furthermore, it has been demonstrated[30–32] that in lattice-mismatched zinc-blende heterostructures, interface roughness gives rise to fluctuations in the strain. The effects of strain fluctuations are, in general, twofold. First, these produce a fluctuating density of bulk piezoelectric charges in the strained layer.[31–33] Recently, Quang and co-workers[34] have extended this idea to wurtzite III-nitride heterostructures. They found that because of interface roughness there must exist fluctuating densities of bulk piezoelectric charges inside of the strained and relaxed layers as well as of sheet piezoelectric charges on the interface. In view of the fact that the nitrides generally possess strong piezoelectricity and large lattice mismatch, we expect that these roughness-induced charges are an important scattering source.

Second, it has been shown[30,33] that strain fluctuations produce random nonuniform variations of the band edges of the conduction and valence bands. These act as perturbating potentials on electrons and holes, so scattering the charge carriers and limiting their mobility.

The roughness-induced piezoelectric and deformation potential scatterings are new effects in the area of the transport theory of wurtzite III-nitride heterostructures. However, up to now these have not been included in the calculations of their electron mobility.[8,11,12,14–18]

Thus, the goal of the present paper is to develop a theory of the low-temperature mobility of electrons in wurtzite III-nitride heterostructures, taking account of the above roughness-related scattering mechanisms and the effect arising from sheet polarization charges. While there have been in the existing literature[18,19,27–29] merely numerical solutions, we propose an analytic approach to the polarization confinement effect, so obtaining an explicit description of the influence of sheet polarization charges on the screening as well as the unscreened and screened scattering potentials.

The paper is organized as follows. In Sec. II below, we derive an analytic solution to the electron wave function in a triangular quantum well (QW), allowing for the effects from both the finiteness of the potential barrier height and the polarization confinement. In Sec. III, we provide the basic equations to calculate the low-temperature disorder-limited 2DEG mobility. In Sec. IV, the autocorrelation functions for diverse scattering mechanisms are derived. Section V is devoted to numerical results and conclusions with reference to recent experiments on the SH and DH samples. Finally, a summary is given in Sec. VI.

II. POLARIZATION EFFECT ON THE QUANTUM CONFINEMENT

A. Density of sheet polarization-induced charges

In what follows, as a representative of wurtzite group-III-nitride heterostructures we will be dealing with an AlGaN/GaN sample, which are composed of an AlGaN layer grown pseudomorphically on a GaN layer. The crystal reference system is such that the z axis is opposite to the growth direction [0001], and $z=0$ defines the interface plane between the AlGaN barrier ($z<0$) and the GaN well ($z>0$). It is assumed that the AlGaN layer be under tensile strain, while the GaN layer be relaxed. The constituents of the system are labeled by such a layer index that $\lambda=$b and w refer to the barrier and well layers, respectively.

It is well known[25,26] that if the AlGaN/GaN interface of the sample is absolutely flat, the piezoelectric and spontaneous polarizations in each layer are uniform. The total polarization is subjected to an abrupt change across the interface plane. This induces a uniform density of positive sheet charges bound on the interface, which is a function of the Al content x, given by[10,35]

$$\sigma = 0.052x + 2\epsilon_{\parallel}\left(e_{31}^{\mathrm{b}} - e_{33}^{\mathrm{b}}\frac{c_{13}^{\mathrm{b}}}{c_{33}^{\mathrm{b}}}\right) \tag{1}$$

(in units of $\mathrm{C/m^2}$). Hereafter, c_{ij}^{λ} and e_{ij}^{λ} are the elastic stiffness and piezoelectric constants of the λ layer ($\lambda=$b,w). The lattice mismatch is defined by

$$\epsilon_{\parallel} = \frac{a(0)-a(x)}{a(x)}, \tag{2}$$

with $a(x)$ and $a(0)$ as the lattice constants of the free-standing AlGaN and GaN, respectively. It is to be noted that in addition to $\epsilon_{\parallel}$ increasing with x, the constants c_{ij}^{b} and e_{ij}^{b} also vary with x.

The above sheet polarization charges create a uniform normal electric field. Thus, this can squeeze the electron wave function along the growth direction rather than affect the free 2D motion of electrons in the in-plane, so presenting no scattering source of the 2DEG.

It should be noted that up to now, the polarization confinement effect on the scattering processes in wurtzite III-nitride heterostructures or, equivalently, on their 2DEG mobility has hardly been examined. A thorough study of this is, therefore, of obvious interest.

B. Polarization confinement effect

The electrons moving along the in-plane are scattered by various sources of disorder, which are normally characterized by some random fields. It is well known[36] that scattering by a Gaussian random field is specified by its autocorrelation function in wave vector space $\langle|U(\mathbf{q})|^2\rangle$. Hereafter, the angular brackets stand for an ensemble average. $U(\mathbf{q})$ is a 2D Fourier transform of the unscreened scattering potential averaged with the envelope wave function of a 2D subband:

$$U(\mathbf{q}) = \int_{-\infty}^{+\infty} dz|\zeta(z)|^2 U(\mathbf{q},z). \tag{3}$$

As usual,[14,37] for the electrons confined in the channel layer, we assume a triangular QW located along the growth direction. It was indicated[38–40] that the potential barrier height may play an important role in certain phenomena. For the triangular QW in an AlGaN/GaN heterostructure, Poisson-Schrödinger simulations[18,19] revealed that the electron distribution has a significant penetration depth into the barrier. Therefore, we must, in general, adopt the realistic model of finitely deep wells.

The 2DEG is assumed to primarily occupy the lowest subband. It has been shown[38–40] that for a finitely deep tri-

angular QW, this may be very well described by a modified Fang-Howard wave function, proposed by Ando[38]

$$\zeta(z) = \begin{cases} A\kappa^{1/2}\exp(\kappa z/2), & \text{for } z < 0, \\ Bk^{1/2}(kz + c)\exp(-kz/2), & \text{for } z > 0, \end{cases} \tag{4}$$

in which A, B, c, k, and κ are variational parameters to be determined. Here, k and κ are half the wave numbers in the well and the barrier, respectively. A, B, and c are dimensionless parameters given in terms of k and κ through boundary conditions at the interface plane $z=0$ and the normalization. These read[39,40]

$$A\kappa^{1/2} = Bk^{1/2}c, \quad A\kappa^{3/2}/2 = Bk^{3/2}(1 - c/2),$$

$$A^2 + B^2(c^2 + 2c + 2) = 1. \tag{5}$$

As for the confinement of an electron along the growth direction, its total potential energy may be written as a sum of two terms:

$$V_{\text{tot}}(z) = V_{\text{b}}(z) + V_{\text{H}}(z), \tag{6}$$

where $V_{\text{b}}(z)$ is the barrier potential, and $V_{\text{H}}(z)$ is the Hartree potential. The former is of some finite height V_0. In a doped sample the latter is specified by the density of acceptors $N_{\text{A}}(z)$ and donors $N_{\text{D}}(z)$, the sheet density of confined electrons n_{s} and, in addition, by the areal density of sheet polarization charges σ/e, according to the Poisson equation[39,40]

$$\frac{d^2}{dz^2}V_{\text{H}}(z) = -\frac{4\pi e^2}{\varepsilon_{\text{L}}}\left[N_{\text{A}}(z) - N_{\text{D}}(z) + n_{\text{s}}|\zeta(z)|^2 - \frac{\sigma}{e}\delta(z)\right], \tag{7}$$

where ε_{L} is the dielectric constant of the sample, neglecting a small difference in its values between the layers with the use of an average value.

The acceptor and donor densities in a modulation doping of the barrier layer are given as follows:

$$N_{\text{A}}(z) - N_{\text{D}}(z) = \begin{cases} N_{\text{d}}/z_{\text{d}}, & \text{for } 0 < z < z_{\text{d}}, \\ -N_{\text{I}}, & \text{for } -(L_{\text{s}} + L_{\text{d}}) < z < -L_{\text{s}}, \\ 0, & \text{elsewhere}. \end{cases} \tag{8}$$

Here, N_{d} is the density of depletion charges, and z_{d} the depletion layer thickness. N_{I} is the density of ionized impurities and L_{d} and L_{s} are the thicknesses of the doped and spacer layers, respectively.

The energy of the ground-state subband is calculated as a function of the wave numbers k and κ such that[39,40]

$$\begin{aligned} E_0(k,\kappa) = &-\frac{\hbar^2}{8m_z}[B^2k^2(c^2 - 2c - 2) + A^2\kappa^2] + V_0A^2 \\ &+ \frac{4\pi e^2N_{\text{d}}}{\varepsilon_{\text{L}}}\left[\frac{B^2}{k}(c^2 + 4c + 6) - \frac{A^2}{\kappa}\right] + \frac{4\pi e^2n_{\text{s}}}{\varepsilon_{\text{L}}} \\ &\times\left[\frac{B^4}{4k}(2c^4 + 12c^3 + 34c^2 + 50c + 33) + \frac{A^4}{2\kappa} - \frac{A^2}{\kappa}\right] \\ &+ \frac{4\pi e^2N_{\text{I}}}{\varepsilon_{\text{L}}}\frac{A^2}{\kappa^2}e^{-\kappa L_{\text{s}}}(1 - e^{-\kappa L_{\text{d}}}) \\ &+ \frac{2\pi e\sigma}{\varepsilon_{\text{L}}}\left[\frac{B^2}{k}(c^2 + 4c + 6) + \frac{A^2}{\kappa}\right], \end{aligned} \tag{9}$$

where $m_z = 0.18m_{\text{e}}$ is the effective electron mass of the GaN in the growth direction.[41] The wave numbers k and κ are to be fixed so as to minimize the total energy per electron $E(k,\kappa)$ numerically.[38–40]

The peak of the electron distribution along the growth direction is normally located at the expectation value of its z coordinate, given by[39]

$$\bar{z} = \frac{B^2}{k}(c^2 + 4c + 6) - \frac{A^2}{\kappa}. \tag{10}$$

The size of the distribution is estimated to be $2\bar{z}$.[36]

We are now examining the effect of sheet polarization charges on the quantum confinement. For simplicity, we consider the limiting case of $V_0 \to \infty$. It holds that $A \propto V_0^{-1/2} \to 0$, $B = 1/\sqrt{2}$, $c = 0$, and $\kappa \propto V_0^{1/2} \to \infty$. Then, Eq. (9) reproduces the lowest-subband energy for an infinitely deep well described by the standard Fang-Howard wave function.[36] Moreover, half the size of the electron distribution is simplified to

$$\bar{z} = 3/k, \tag{11}$$

where

$$k = \left\{\frac{48\pi m_z e^2}{\hbar^2\varepsilon_{\text{L}}}\left[N_{\text{d}} + \frac{11}{32}n_{\text{s}} + \frac{1}{2}\frac{\sigma}{e}\right]\right\}^{1/3}. \tag{12}$$

This expression for the well wave number k is clearly distinguished from the well-known formula[36] by the presence of the last term $(\sigma/e)/2$ on the right-hand side. Thus, it is seen from Eqs. (11) and (12) that the electron distribution is fixed not only by the density of electrons and depletion charges but also the density of sheet polarization charges. In the case of $\sigma/e \gg n_{\text{s}}, N_{\text{d}}$, its size is reduced mainly by increasing the last: $\bar{z} \propto 1/\sigma^{1/3}$.

It is interesting to mention that while there has so far been in the literature merely computational estimation,[18,19,27–29] Eq. (12) enables a simple analytic evaluation of the polarization confinement effect on the electron distribution in the well.

The shift of its peak is

$$\Delta\bar{z} = \bar{z} - \bar{z}_0, \tag{13}$$

where the subindex 0 means the absence of sheet polarization charges ($\sigma = 0$).

As usual, $N_{\text{d}} \ll n_{\text{s}}, \sigma/e$, with the aid of Eqs. (11) and (12) we immediately obtain

$$\Delta\bar{z} = \left(\frac{54}{33}\frac{\hbar^2\varepsilon_{\text{L}}}{\pi m_z e^2 n_{\text{s}}}\right)^{1/3}\left[\left(1 + \frac{\sigma/e}{n_{\text{s}}}\right)^{-1/3} - 1\right]. \tag{14}$$

Therefore, $\Delta\bar{z} < 0 : \bar{z} < \bar{z}_0$, so the peak of the electron distribution is shifted toward the interface plane. For instance, for a 300 Å $Al_{0.15}Ga_{0.85}N$ barrier, we have $n_{\text{s}} \sim 6.5 \times 10^{12}$ cm^{-2} and $\sigma/e \sim 8 \times 10^{12}$ cm^{-2}.[35] The relative shift is $|\Delta\bar{z}|/\bar{z}_0 \sim 23.4\%$.

III. LOW-TEMPERATURE ELECTRON MOBILITY

In what follows, we are concerned with wurtzite III-nitride heterostructures, e.g., AlGaN/GaN at very low temperature. The electron mobility may be then determined within the relaxation time approximation by

$$\mu = e\tau/m^*, \tag{15}$$

in which $m^*=0.228m_e$ is the effective in-plane electron mass of the GaN.[42]

It was indicated[43] that the sheet polarization charges in an AlGaN/GaN heterostructure may enable a 2DEG of very high density ($n_s \sim 10^{13}$ cm^{-2}). Under such a high carrier density the multiple scattering effects were found[44,45] to be negligibly weak, so that we may adopt the linear transport theory as a good approximation. The inverse relaxation time for zero temperature is then expressed in terms of the autocorrelation function for each disorder:[46,47]

$$\frac{1}{\tau} = \frac{1}{2\pi\hbar E_F}\int_0^{2k_F} dq \frac{q^2}{(4k_F^2 - q^2)^{1/2}} \frac{\langle |U(\mathbf{q})|^2 \rangle}{\varepsilon^2(q)}. \tag{16}$$

Here $q=|\mathbf{q}|$, with $\mathbf{q}$ as a 2D wave vector in the interface plane, $E_F=\hbar^2k_F^2/2m^*$ is the Fermi energy with k_F as the Fermi wave number fixed by the electron density $k_F=\sqrt{2\pi n_s}$.

At very low temperature, the carriers are assumed to primarily occupy the ground-state subband, and the scattering processes limiting their mobility occur mainly within this subband. Thus, the autocorrelation function $\langle |U(\mathbf{q})|^2 \rangle$ entering Eq. (16) is supplied by Eq. (3) for an unscreened scattering potential with the lowest-subband wave function from Eq. (4).

The dielectric function $\varepsilon(q)$ figuring in Eq. (16) allows for the screening of scattering potentials by the 2DEG. Within the random phase approximation, this is given at zero temperature by[36]

$$\varepsilon(q) = 1 + \frac{q_{TF}}{q} F_S(q/k)[1 - G(q)] \quad \text{for } q \leqslant 2k_F, \tag{17}$$

with $q_{TF}=2m^*e^2/\varepsilon_L\hbar^2$ as the inverse 2D Thomas-Fermi screening length.

The screening form factor $F_S(q/k)$ in Eq. (17) accounts for the extension of the electron distribution along the growth direction. With the use of the lowest-subband wave function from Eq. (4), this is estimated to be[40]

$$F_S(t) = \frac{A^4 a}{t+a} + 2A^2B^2a\frac{2 + 2c(t+1) + c^2(t+1)^2}{(t+a)(t+1)^3} + \frac{B^4}{2(t+1)^3}[2(c^4 + 4c^3 + 8c^2 + 8c + 4) + t(4c^4 + 12c^3 + 18c^2 + 18c + 9) + t^2(2c^4 + 4c^3 + 6c^2 + 6c + 3)]. \tag{18}$$

Here, we introduced the dimensionless wave numbers in the interface plane (t) and the barrier (a) by definition

$$t = q/k, \quad a = \kappa/k. \tag{19}$$

In the limiting case of $V_0 \to \infty$, this is simplified to the well-known expression[36]

$$F_S(t) = \frac{3t^2 + 9t + 8}{8(t+1)^3}. \tag{20}$$

This reveals that the screening form factor is increased with a decrease of t and, hence, with an increase of the well wave number k. According to Eq. (12), the screening effect is enhanced when elevating not only the densities of electrons and depletion charges but also that of sheet polarization charges. At a high value of the last, the 2DEG screening is strongly enhanced by the polarization confinement.

Finally, the function $G(q)$ appears in Eq. (17) to allow for the local field corrections associated with the many-body interaction in the 2DEG. Within Hubbard's approximation, in which merely the exchange effect is included, it holds[48]

$$G(q) = \frac{q}{2(q^2 + k_F^2)^{1/2}}. \tag{21}$$

At very low temperature the phonon scattering is negligibly weak. Therefore, the electrons in a doped sample are expected to experience the following possible sources of scattering: (i) ionized dopants, (ii) alloy disorder, (iii) surface roughness, (iv) roughness-induced piezoelectric charges, and (v) roughness-induced deformation potential. The total relaxation time is then determined by the ones for individual disorders according to Matthiessen's rule:

$$\frac{1}{\tau_{tot}} = \frac{1}{\tau_{ID}} + \frac{1}{\tau_{AD}} + \frac{1}{\tau_{SR}} + \frac{1}{\tau_{PE}} + \frac{1}{\tau_{DP}}. \tag{22}$$

IV. AUTOCORRELATION FUNCTIONS FOR SCATTERING MECHANISMS

A. Ionized dopants

As evidently seen from Eq. (16), in our calculation of the disorder-limited 2DEG mobility the autocorrelation function in wave vector space $\langle |U(\mathbf{q})|^2 \rangle$ takes a key role. Thus, we ought to specify it for the abovementioned scattering mechanisms.

To start with, we are examining scattering by ionized dopants. The autocorrelation function for scattering by randomly distributed charged impurities is shown[36,47] to be represented in the form

$$\langle |U_{ID}(\mathbf{q})|^2 \rangle = \left(\frac{2\pi e^2}{\varepsilon_L q}\right)^2 \int_{-\infty}^{+\infty} dz_i N_I(z_i) F_R^2(q, z_i). \tag{23}$$

Here, $N_I(z_i)$ is the three-dimensional impurity density, and for a modulation doping of the barrier layer: $N_I(z_i)=N_I$ for $-(L_s+L_d)<z_i<-L_s$, and is zero elsewhere. $F_R(q,z_i)$ denotes the form factor for a sheet of impurities located in the plane $z=z_i$ and accounts for the extension of the electron state along the growth direction, given by

$$F_R(q, z_i) = \int_{-\infty}^{+\infty} dz |\zeta(z)|^2 e^{-q|z-z_i|}. \tag{24}$$

Nevertheless, it has been experimentally indicated[49] that the assumption of the random impurity distribution fails to be valid at high doping levels, and for the understanding of several observable properties of heavily doped semiconductor systems one has to allow for high-temperature ionic correlation. This is due to Coulomb interactions between the charged impurities in their diffusion during growth and tends to reduce the probability for large fluctuations in their density and, hence, in their potential, so reducing the autocorrelation function. Thus, the ionic correlation may be referred to as a statistical screening and weakens the impurity scattering, so increasing the respective partial mobility.[50,51]

It was shown[52] that for taking into account the ionic correlation, we have to incorporate an appropriate correlation factor (less than unity) into the autocorrelation function as follows:

$$\langle |U_{\mathrm{ID}}(\mathbf{q})|^2 \rangle_{\mathrm{c}} = \langle |U_{\mathrm{ID}}(\mathbf{q})|^2 \rangle \frac{q}{q+q_{\mathrm{i}}}. \tag{25}$$

Here, the angular brackets with subindex c means the ensemble average over the correlated impurity distribution, and q_{i} is the inverse statistical-screening radius, given by

$$q_{\mathrm{i}} = \frac{2\pi e^2 n_{\mathrm{i}}}{\varepsilon_{\mathrm{L}} k_{\mathrm{B}} T_0}, \tag{26}$$

where $n_{\mathrm{i}}=N_{\mathrm{I}}L_{\mathrm{d}}$ is the 2D impurity density, and T_0 the freezing temperature for impurity diffusion ($\sim$1000 K).

Additionally, it should be noticed that the positive sheet polarization charges of high density are localized in a very thin AlGaN region of thickness measured from the interface plane $L_\sigma \sim 6$ Å.[18,35,53] Because of their Coulomb repulsions, the positive-charged impurities in diffusion cannot penetrate into this region. Thus, in the case of n-type doping of the barrier there must invariably exist a spacer layer of thickness $L_{\mathrm{s}} \geqslant L_\sigma$.

With the use of the lowest-subband wave function from Eq. (4), we may find the autocorrelation function for scattering by correlated ionized dopants in the form

$$\begin{aligned}\langle |U_{\mathrm{ID}}(\mathbf{q})|^2 \rangle_{\mathrm{c}} = {} & \left(\frac{2\pi e^2}{\varepsilon_{\mathrm{L}}}\right)^2 \frac{N_{\mathrm{I}}}{2q^2(q+q_{\mathrm{i}})} e^{-2st} \\ & \times \left\{ A^4 \frac{a^2}{(t-a)^2} \left[1 - e^{-2dt} - \frac{8t^2}{(t+a)^2} e^{s(t-a)} \right.\right. \\ & \times (1 - e^{-d(t+a)}) + \frac{4t^3}{a(t+a)^2} e^{2s(t-a)} (1 - e^{-2da}) \Big] \\ & - 2A^2B^2 \frac{a}{t-a} \left[\frac{2}{(t+1)^3} + \frac{2c}{(t+1)^2} + \frac{c^2}{t+1} \right] \\ & \times \left[1 - e^{-2dt} - \frac{4t^2}{(t+a)^2} e^{s(t-a)} (1 - e^{-d(t+a)}) \right] \\ & \left. + B^4 \left[\frac{2}{(t+1)^3} + \frac{2c}{(t+1)^2} + \frac{c^2}{t+1} \right]^2 (1 - e^{-2dt}) \right\}. \end{aligned} \tag{27}$$

Here, in addition to the dimensionless wave numbers from Eq. (19), we introduced the dimensionless thicknesses for the doped (d) and spacer (s) layers by definition

$$d = kL_{\mathrm{d}}, \quad s = kL_{\mathrm{s}}. \tag{28}$$

In the limiting case of $V_0 \to \infty$, this is simplified to

$$\langle |U_{\mathrm{ID}}(\mathbf{q})|^2 \rangle_{\mathrm{c}} = \left(\frac{2\pi e^2}{\varepsilon_{\mathrm{L}}}\right)^2 \frac{N_{\mathrm{I}}}{2q^2(q+q_{\mathrm{i}})} \frac{e^{-2st}(1-e^{-2dt})}{(t+1)^6}. \tag{29}$$

Equation (29) reveals that the autocorrelation function is increased with a rise of the well wave number k and, according to Eq. (12), with a rise of sheet polarization charges. Thus, the unscreened potential for impurity scattering is enhanced by polarization confinement.

In what follows, as a measure of the polarization confinement effect on a scattering source, we consider the ratio of its autocorrelation functions in the presence and in the absence of sheet polarization charges

$$R^{\mathrm{uns}} = \frac{\langle |U(\mathbf{q},\sigma)|^2 \rangle}{\langle |U(\mathbf{q},\sigma=0)|^2 \rangle}, \tag{30}$$

which is, for short, called the polarization ratio for its unscreened potential.

Upon putting Eq. (29) into Eq. (30), for impurity scattering we immediately obtain

$$R_{\mathrm{ID}}^{\mathrm{uns}} = \left(\frac{k}{k_0} \frac{q+k_0}{q+k} \right)^6, \tag{31}$$

with $k_0=k(\sigma=0)$. Since $k_0<k$, the ratio is larger than unity and exhibits an increasing function of the in-plane wave number q.

Under $N_{\mathrm{d}} \ll n_{\mathrm{s}}$, σ/e, we have the limiting values

$$R_{\mathrm{ID}}^{\mathrm{uns}} = \begin{cases} 1, & \text{for } q \ll k, k_0, \\ \left(1 + \dfrac{16}{11} \dfrac{\sigma/e}{n_{\mathrm{s}}}\right)^2, & \text{for } q \gg k, k_0. \end{cases} \tag{32}$$

For $\sigma/e \sim n_{\mathrm{s}}$, $R_{\mathrm{ID}}^{\mathrm{uns}} \sim 6$ for large q. Thus, the unscreened impurity potential at a small q is weakly influenced by sheet polarization charges, but at a large q drastically enhanced by their large density.

B. Alloy disorder

The autocorrelation function for scattering by alloy disorder located in the AlGaN barrier is supplied by[38,39]

$$\langle |U_{\mathrm{AD}}(\mathbf{q})|^2 \rangle = x(1-x) u_{\mathrm{al}}^2 \Omega \int_{-L_{\mathrm{b}}}^{0} dz \zeta^4(z), \tag{33}$$

where x is, as before, the Al content of the alloy layer, L_{b} is its thickness, and u_{al} is the alloy potential assumed[39] to be close to the conduction band offset between AlN and GaN: $u_{\mathrm{al}} \approx \Delta E_{\mathrm{c}}(1) = 2.03$ eV. The volume of a hexagonal unit cell is given by $\Omega = \sqrt{3} a^2(x) c(x)/2$, with $a(x)$ and $c(x)$ as the lattice constants of the alloy.[54]

By means of Eq. (4) for the lowest-subband wave function, this is written in terms of the barrier wave number κ as follows:

$$\langle |U_{\mathrm{AD}}(\mathbf{q})|^2 \rangle = x(1-x)u_{\mathrm{al}}^2 \Omega \frac{A^4 \kappa}{2}(1-e^{-2\kappa L_{\mathrm{b}}}). \quad (34)$$

In the limiting case of $V_0 \to \infty$: $A^4\kappa \to 0$, the alloy disorder scattering becomes vanishing, the 2DEG being spatially separated from the alloy.

C. Surface roughness

Next, we treat the scattering of confined charge carriers from a rough potential barrier of a finite height V_0. The scattering potential is due to fluctuations in the position of the barrier. The average scattering potential in wave vector space is fixed by the value of the envelope wave function at the barrier plane according to[36]

$$U_{\mathrm{SR}}(\mathbf{q}) = V_0 |\zeta(0)|^2 \Delta_{\mathbf{q}}, \quad (35)$$

where $\Delta_{\mathbf{q}}$ denotes a Fourier transform of the interface roughness profile.

To estimate the average potential for surface scattering specified by Eq. (35) with the use of a variational wave function, we are to adopt the relation[33]

$$V_0 |\zeta(0)|^2 = \int_0^\infty dz |\zeta(z)|^2 \frac{\partial V_{\mathrm{H}}(z)}{\partial z}, \quad (36)$$

where $V_{\mathrm{H}}(z)$ is, as before, the Hartree potential satisfying Eq. (7). It is to be noted that Eq. (36) is exact and applicable for any value of the barrier height V_0.

Upon making use of Eqs. (7) and (36) with the lowest-subband wave function from Eq. (4), we obtain

$$V_0 |\zeta(0)|^2 = \frac{4\pi e^2}{\varepsilon_{\mathrm{L}}} \left\{ B^2 \left[N_{\mathrm{d}}(c^2+2c+2) + \frac{1}{2} n_{\mathrm{s}} B^2 (c^4+4c^3+8c^2+8c+4) \right] + \frac{1}{2}\frac{\sigma}{e}(1-A^2) \right\}. \quad (37)$$

Thus, with the help of Eqs. (35) and (37), we may arrive at the following autocorrelation function for surface roughness scattering in finitely deep triangular QWs:

$$\langle |U_{\mathrm{SR}}(\mathbf{q})|^2 \rangle = \left(\frac{4\pi e^2}{\varepsilon_{\mathrm{L}}} \right)^2 \left\{ B^2 \left[N_{\mathrm{d}}(c^2+2c+2) + \frac{1}{2} n_{\mathrm{s}} B^2 (c^4+4c^3+8c^2+8c+4) \right] + \frac{1}{2}\frac{\sigma}{e}(1-A^2) \right\}^2 \langle |\Delta_{\mathbf{q}}|^2 \rangle. \quad (38)$$

For $V_0 \to \infty$, this is reduced to a simple expression

$$\langle |U_{\mathrm{SR}}(\mathbf{q})|^2 \rangle = \left(\frac{4\pi e^2}{\varepsilon_{\mathrm{L}}} \right)^2 \left(N_{\mathrm{d}} + \frac{1}{2} n_{\mathrm{s}} + \frac{1}{2}\frac{\sigma}{e} \right)^2 \langle |\Delta_{\mathbf{q}}|^2 \rangle. \quad (39)$$

It is obvious that the last term on the right-hand side of Eqs. (38) and (39) describes the effect from polarization confinement on surface roughness scattering. This shows up in a quadratic dependence on the density of sheet polarization charges.

Upon inserting Eq. (39) into Eq. (30) and neglecting depletion charges, the polarization ratio for surface roughness scattering reads

$$R_{\mathrm{SR}}^{\mathrm{uns}} = \left(1 + \frac{\sigma/e}{n_{\mathrm{s}}} \right)^2. \quad (40)$$

One has an estimation $R_{\mathrm{SR}}^{\mathrm{uns}} \sim 1$ for $\sigma/e \ll n_{\mathrm{s}}$ and $R_{\mathrm{SR}}^{\mathrm{uns}} \sim 4$ for $\sigma/e \sim n_{\mathrm{s}}$. Thus, the unscreened potential for surface roughness scattering is weakly influenced by sheet polarization charges at their low density, but drastically enhanced at their high density.

D. Roughness-induced piezoelectric charges

As mentioned before, in wurtzite III-nitride heterostructures, e.g., AlGaN/GaN, surface roughness gives rise to strain fluctuations in both strained and relaxed layers. In Ref. 34 we have demonstrated that the strain fluctuations produce random nonuniform variations in the piezoelectric polarization. These in turn induce fluctuating densities of piezoelectric charges, viz., bulk charges inside of the strained and relaxed layers as well as sheet charges on the interface. The charges create relevant electric fields and act as scattering sources on the 2D motion of electrons in the in-plane.

It have been pointed out[34] that the average electric field due to sheet charges is much weaker than those of bulk charges. In addition, the average field due to bulk charges in the GaN well is nearly equal to that in the AlGaN barrier. Thus, the effect from the former is remarkably stronger than that from the latter since the 2DEG is located mainly in the same space region as the former. Therefore, we may plausibly restrict ourselves to calculate the scattering by bulk charges located in the well layer.

The potential energy for an electron moving in the field due to roughness-induced bulk piezoelectric charges in the channel layer is described by a simple 2D Fourier transform as follows:[34]

$$U_{\mathrm{PE}}(\mathbf{q},z) = \frac{\pi \alpha \epsilon_{\parallel} e Q}{\varepsilon_{\mathrm{L}}} q \Delta_{\mathbf{q}} F_{\mathrm{PE}}(q,z). \quad (41)$$

Here, α denotes the anisotropy ratio as a measure for the deviation of hexagonal symmetry of the wurtzite crystal from isotropy, $\epsilon_{\parallel}$ is the lattice mismatch from Eq. (2). We introduced a material parameter characteristic of the well, defined in terms of its elastic stiffness c_{ij}^{w} and piezoelectric e_{ij}^{w} constants by

$$Q = \frac{C_{\mathrm{b}}}{c_{33}^{\mathrm{b}}} \left[\frac{e_{15}^{\mathrm{w}}}{c_{44}^{\mathrm{w}}} + \frac{e_{31}^{\mathrm{w}}(c_{33}^{\mathrm{w}}+2c_{13}^{\mathrm{w}}) - e_{33}^{\mathrm{w}}(c_{11}^{\mathrm{w}}+c_{12}^{\mathrm{w}}+c_{13}^{\mathrm{w}})}{C_{\mathrm{w}}} \right], \quad (42)$$

with

$$C_{\lambda} = c_{33}^{\lambda}(c_{11}^{\lambda}+c_{12}^{\lambda}) - 2(c_{13}^{\lambda})^2, \quad (43)$$

$(\lambda = \mathrm{b}, \mathrm{w})$.

The form factor figuring in Eq. (41) is given by

$$F_{\mathrm{PE}}(q,z) = \frac{1}{2q} \begin{cases} e^{qz}, & \text{for } z \leqslant 0, \\ e^{-qz}(1+2qz), & \text{for } z > 0. \end{cases} \quad (44)$$

It is clearly seen from Eq. (41) that Q may be regarded as an "effective" piezoelectric constant which quantifies the action of bulk charges in the well on the electron.

Upon averaging Eqs. (41) and (44) by means of the lowest-subband wave function from Eq. (4), we obtain the weighted potential for scattering by roughness-induced piezoelectric charges:

$$U_{\mathrm{PE}}(\mathbf{q}) = \frac{\pi\alpha\epsilon_{\|}eQ}{\varepsilon_{\mathrm{L}}} F_{\mathrm{PE}}(q/k)\Delta_{\mathbf{q}}. \tag{45}$$

The weighted piezoelectric form factor in Eq. (45) is expressed as a function of the dimensionless wave numbers in Eqs. (19):

$$F_{\mathrm{PE}}(t) = \frac{A^2}{2}\frac{a}{t+a} + \frac{B^2}{2}\left\{\frac{2}{(t+1)^3} + \frac{2c}{(t+1)^2} + \frac{c^2}{t+1} + 2t\left[\frac{6}{(t+1)^4} + \frac{4c}{(t+1)^3} + \frac{c^2}{(t+1)^2}\right]\right\}. \tag{46}$$

In the limiting case of $V_0 \to \infty$, this is simplified to

$$F_{\mathrm{PE}}(t) = \frac{1}{2(t+1)^3} + \frac{3t}{(t+1)^4}. \tag{47}$$

E. Roughness-induced deformation potential

As quoted before, roughness-induced strain fluctuations give rise to random nonuniform shifts of the band edges.[30–33] This implies that electrons in the conduction band and holes in the valence one must experience a perturbating potential. The roughness-induced deformation potential for the electron is determined by fluctuations of a diagonal strain component, $\Delta\epsilon_{zz}$, according to (see Refs. 55 and 56)

$$U_{\mathrm{DP}} = \Xi_{\mathrm{d}}\Delta\epsilon_{zz}, \tag{48}$$

where Ξ_{d} is the combined dilational component of the deformation potential for the conduction band. Since the deformation potential is of short range, and the 2DEG is located mainly in the well, we can reasonably take into account the relevant scattering merely in this layer.

On the substitution of roughness-induced fluctuations of the strain in the well, which were derived in Ref. 34, into Eq. (48), we readily get a 2D Fourier transform of the perturbating potential for the electron as follows:

$$U_{\mathrm{DP}}(\mathbf{q},z) = \frac{\alpha\epsilon_{\|}\Xi_{\mathrm{d}}}{2}\frac{C_{\mathrm{b}}}{c_{33}^{\mathrm{b}}}\frac{c_{11}^{\mathrm{w}} + c_{12}^{\mathrm{w}} + c_{13}^{\mathrm{w}}}{C_{\mathrm{w}}} q\,\Delta_{\mathbf{q}} e^{-qz}, \tag{49}$$

for $z \geqslant 0$, and is zero elsewhere. Here, c_{ij}^{λ} are, as above, the elastic stiffness constants of the λ layer, and C_{λ} defined by Eq. (43).

Upon averaging Eq. (49) by means of the lowest-subband wave function from Eq. (4), we may represent the autocorrelation function for deformation potential scattering in the form

$$\langle|U_{\mathrm{DP}}(\mathbf{q})|^2\rangle = \left\{\frac{\alpha\epsilon_{\|}\Xi_{\mathrm{d}}}{2}\frac{C_{\mathrm{b}}}{c_{33}^{\mathrm{b}}}\frac{c_{11}^{\mathrm{w}} + c_{12}^{\mathrm{w}} + c_{13}^{\mathrm{w}}}{C_{\mathrm{w}}} q F_{\mathrm{DP}}(q/k)\right\}^2 \langle|\Delta_{\mathbf{q}}|^2\rangle, \tag{50}$$

where the form factor is given by

$$F_{\mathrm{DP}}(t) = B^2\left[\frac{2}{(t+1)^3} + \frac{2c}{(t+1)^2} + \frac{c^2}{t+1}\right]. \tag{51}$$

In the limiting case of $V_0 \to \infty$, it holds that

$$F_{\mathrm{DP}}(t) = \frac{1}{(t+1)^3}. \tag{52}$$

Upon inserting Eqs. (50) and (52) into Eq. (30), we immediately obtain a simple relation

$$R_{\mathrm{DP}}^{\mathrm{uns}} = R_{\mathrm{ID}}^{\mathrm{uns}}. \tag{53}$$

This indicates that as in the case of ionized dopants, the unscreened deformation potential is hardly influenced by sheet polarization charges at small in-plane wave number q, but strengthened at large q.

It is clearly observed from Eqs. (45) and (50) that the roughness-related scattering mechanisms, viz., piezoelectric charges and deformation potential, exhibit a quadratic dependence on not only the interface profile but also the lattice mismatch, i.e., the residual strain in the barrier layer. As a result, these are enhanced with an increase of the lattice mismatch, i.e., according to Eq. (2), with an increase of the alloy content.

To end this section, we may conclude that within the realistic model of finitely deep triangular QWs described by the modified Fang-Howard wave function (4), we have rigorously derived the autocorrelation functions, i.e., the scattering rates in an analytic form for the diverse scattering mechanisms of interest. These are supplied by Eqs. (27), (34), (38), (45), and (50) for scatterings by ionized dopants, alloy disorder, surface roughness, piezoelectric charges, and deformation potential, respectively.

It should be emphasized that in sharp contrast to the earlier theories,[8,11,12,14–17] our mobility calculation, starting from the above-derived autocorrelation functions, properly involves the important effect from sheet polarization charges on the quantum confinement.

V. RESULTS AND CONCLUSIONS

A. Input material parameters

In this section, we are trying to apply the foregoing theory to understand transport properties of the 2DEG in wurtzite III-nitride heterostructures. In particular, we are aiming at the explanation of recent experimental data[12,19] about the low-temperature high-density mobility of the 2DEG in GaN as the conduction channel in strained AlGaN/GaN single and double heterostructures.

For numerical results, we have to specify parameters appearing in the theory as input. The lattice constant, elastic stiffness constants, piezoelectric constants, and dielectric constant for AlN and GaN are taken from Refs. 35 and 57, and listed in Table I. There, the piezoelectric constants are opposite in sign to the ones used in this paper. The corresponding constants for an AlGaN alloy are estimated within the virtual crystal approximation.[35]

We are now examining the potential barrier height V_0 in an AlGaN/GaN heterostructure. This is specified by the fol-

TABLE I. Material parameters used: a and c as the lattice constants (Å), c_{ij} the elastic stiffness constants (GPa), e_{ij} the piezoelectric constants (C/m^2), and ε_L the dielectric constant.

Material	a	c	c_{11}	c_{12}	c_{13}	c_{33}	c_{44}	e_{33}	e_{31}	e_{15}	ε_L
AlN	3.112	4.995	398	142	112	383	118	1.46	−0.60	−0.48	10.1
GaN	3.189	5.237	350	140	104	376	101	0.73	−0.49	−0.3	10.4

lowing facts. As usual, this is assumed to be equal to the conduction band offset between the $Al_xGa_{1-x}N$ barrier and the GaN well, which depends on the Al content x as[58,59]

$$\Delta E_c(x) = 0.75[E_g(x) - E_g(0)], \tag{54}$$

where the band gap of $Al_xGa_{1-x}N$ is measured to be[35]

$$E_g(x) = 6.13x + 3.42(1-x) - x(1-x)\ \text{eV}. \tag{55}$$

However, the potential profile calculation based on the self-consistent solution of Schrödinger's and Poisson's equations reveals[27] an interesting fact that via their Coulomb attractions, positive sheet polarization charges on the interface strongly reduce the penetration depth of the 2DEG into the barrier, which is equivalent to raising its height. For an n-type heavy doping of the barrier, we suggest that positive donors located near to the interface may also strongly reduce the penetration depth, i.e., raise the barrier. In opposite, positive donors outside of the penetration depth lengthen it, i.e., lower the barrier. Thus, the value of V_0 for each sample is to be chosen as a fitting parameter, allowing for the facts in question.

We deal with the choice of the anisotropy ratio α of the wurtzite GaN. For an $Al_{0.25}Ga_{0.75}N/GaN$ sample, the experimental value was determined[60] to be $\alpha_{\text{expt}}=5.56$ and 4.83 for the barrier thickness $L_b=200$ and 400 Å, respectively. Thus, we may accept $\alpha=5$ as a typical value in our numerical calculation.[34]

Next, we turn to the strain deformation potential Ξ_d for the conduction band of wurtzite GaN. It was shown[55,56] that this coupling constant may be deduced from the following empirical relationship:

$$\Xi_d - \left(D_1 - \frac{c_{33}^w}{c_{13}^w} D_2\right) = 38.9\ \text{eV}, \tag{56}$$

where D_1 and D_2 are its deformation potential constants for the valence band. Since there has been in the literature[61–66] a large uncertainty on the values of D_1 and D_2, the conduction band deformation potential is found to be in a wide range from $\Xi_d=14.4$ to 75.0 eV. To estimate the order of the effect, we assume $D_1=-0.89$ eV, $D_2=4.27$ eV,[63] so obtaining $\Xi_d=22.57$ eV as a lower bound for this coupling constant.

Lastly, as seen from Eqs. (38), (45), and (50), the scattering rate from surface roughness, piezoelectric charges, and deformation potential are fixed by the interface profile. Feenstra and co-workers,[67] by measuring the interface morphology of a Si/SiGe heterostructure with the use of atomic force microscopy, indicated that the Fourier spectrum for the surface roughness is well described by a power-law distribution

$$\langle |\Delta(\mathbf{q})|^2 \rangle = \frac{\pi \Delta^2 \Lambda^2}{(1 + q^2\Lambda^2/4n)^{n+1}}. \tag{57}$$

Here, Δ is the roughness amplitude, Λ is a correlation length, and n is an exponent specifying the falloff of the distribution at large in-plane wave numbers. The latter is found in a range from $n=1$ to 4.[30,67] For rather smooth interfaces, we will take the large exponent $n=4$. Thus, Δ and Λ are to be chosen as adjustable parameters for fitting to diverse experiments.

B. Numerical results on the polarization confinement effect

We have carried out numerical calculations of the low-temperature 2DEG mobilities in AlGaN/GaN heterostructures limited by different scattering mechanisms: ionized dopants μ_{ID}, alloy disorder μ_{AD}, surface roughness μ_{SR}, piezoelectric charges μ_{PE}, deformation potential μ_{DP}, and overall mobility μ_{tot}; by employing Eqs. (27), (34), (38), (45), (50), and (22), respectively. For device applications, one is greatly interested in their variation with the sheet density of electrons.

For an apparent illustration of the role of the polarization confinement effect, we have calculated it in the limiting case of an infinitely deep QW, ignoring provisionally the penetration of the 2DEG into the barrier. The effects are both included in the subsequent calculation with reference to the recent experiments.

In Fig. 1, we make a sketch of the standard Fang-Howard

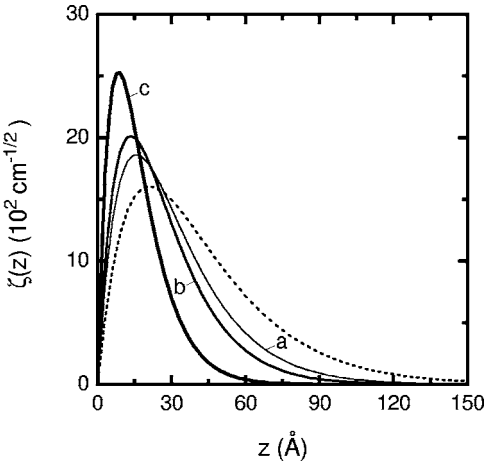

FIG. 1. Standard Fang-Howard wave functions along the growth direction z in the presence (solid line) and the absence (dashed ones) of sheet polarization charges. The solid lines labeled a, b, and c correspond to their densities $\sigma/e=5\times10^{12}$, 1×10^{13} and 5×10^{13} cm^{-2}, respectively.

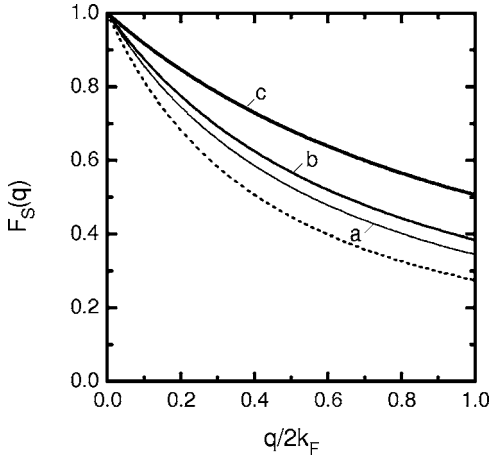

FIG. 2. Screening form factor vs in-plane wave number q in the presence (solid line) and the absence (dashed ones) of sheet polarization charges. The interpretation is the same as in Fig. 1.

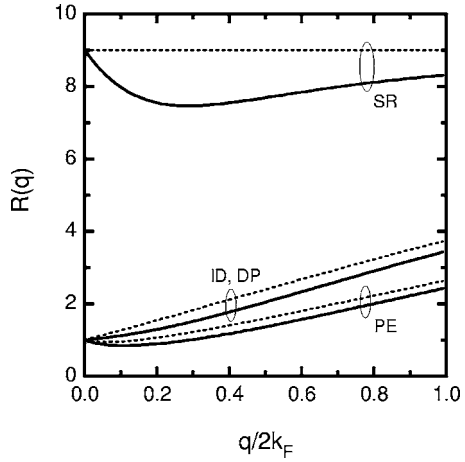

FIG. 3. Ratios between the autocorrelation functions for an infinitely deep QW calculated with and without sheet polarization charges vs in-plane wave number q. The solid and dashed lines correspond to R^{scr} for the screened potential and R^{uns} for the unscreened one, respectively. The lines belong to various scattering mechanisms: ionized dopants (ID), surface roughness (SR), piezoelectric charges (PE), and deformation potential (DP).

wave functions along the growth direction in the presence and the absence of sheet polarization charges, by using Eq. (12) for the well wave number, under a fixed density of electrons $n_s=5\times10^{12}$ cm^{-2} and densities of polarization charges $\sigma/e=5\times10^{12}$, 1×10^{13}, and 5×10^{13} cm^{-2}. In accordance with the wave functions sketched in Fig. 1, the screening form factor from Eq. (20) is plotted in Fig. 2 against the in-plane wave number q (in unit of $q/2k_F$).

As stated previously, the polarization confinement effect on a scattering source is partly described by the ratio R^{uns} [Eq. (30)] of its autocorrelation function, i.e., squared unscreened potential, in the presence of polarization charges to that in their absence. It is clearly observed from Eq. (16) that the net effect on this source is completely described by a ratio of its squared screened potentials, defined by

$$R^{\mathrm{scr}}=\frac{\langle|U(\mathbf{q},\sigma)/\varepsilon(q,\sigma)|^2\rangle}{\langle|U(\mathbf{q},\sigma=0)/\varepsilon(q,\sigma=0)|^2\rangle}. \tag{58}$$

In Fig. 3, the polarization ratios for various scattering mechanisms, except for alloy disorder, are displayed as a function of the in-plane wave number q (in unit of $q/2k_F$) for their screened (solid lines) and unscreened (dashed ones) potentials; by using Eqs. (29), (39), (47), and (52). The densities are fixed at $n_s=5\times10^{12}$ cm^{-2}, and $\sigma/e=1\times10^{13}$ cm^{-2}.

Let us examine the AlGaN (300 Å)/GaN (4000 Å) SH sample studied experimentally in Ref. 12. The doping profile is with a Si donor density $N_I=10^{19}$ cm^{-3}, a thickness of the doped AlGaN layer $L_d=150$ Å, and the spacer $L_s=30$ Å. The roughness profile is with an amplitude $\Delta=2.5$ Å[11] and a correlation length $\Lambda=80$ Å.

In Fig. 4, the partial and overall 2DEG mobilities, exclusive of the alloy disorder one, are plotted versus Al content x in the presence (solid lines) and the absence (dashed ones) of sheet polarization charges. Their density σ is, according to Eq. (1), increased with x, while the carrier density is fixed at $n_s=5\times10^{12}$ cm^{-2}.

From the lines obtained in Figs. 1–4, we may draw the following conclusions.

(i) It is evidently seen from Fig. 1 that owing to positive sheet polarization charges the envelope wave function is, as already quoted, squeezed. The peak of the electron distribution is remarkably narrowered and raised, so pushed closer to the interface plane.

(ii) Figure 2 reveals that the screening form factor becomes larger when the polarization confinement effect is included. This means that the squeeze of the electron wave function enables a noticeable enhancement of the screening. The effect is increased with a rise of the in-plane wave number q.

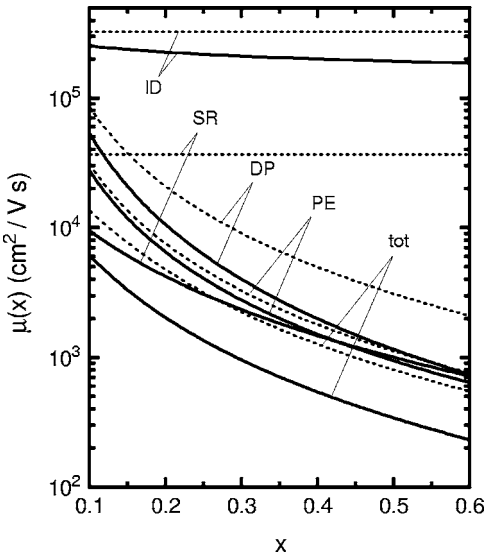

FIG. 4. Different 2DEG mobilities of an AlGaN/GaN SH sample of an infinitely high potential barrier vs Al content x in the presence (solid lines) and the absence (dashed ones) of sheet polarization charges. The lines refer to the mobilities limited by: ionized dopants μ_{ID}, surface roughness μ_{SR}, piezoelectric charges μ_{PE}, deformation potential μ_{DP}, and overall μ_{tot}.

Thus, the polarization charges can cause an enhanced screening in two ways. On one hand, via their electric field they elevate the density of electrons, so enhancing the screening. On the other hand, via the polarization confinement effect they facilitate the redistribution of 2D electrons in the in-plane or, in other words, they elevate the efficiency of the screening act, so enhancing the screening.

(iii) An examination of the dashed lines in Fig. 3 indicates that for the scattering sources such as ionized dopants, surface roughness, and deformation potential, it holds that $R^{\mathrm{uns}}>1$. This is connected with the fact that sheet polarization charges push the 2DEG closer to the sources (or their strongest part), so enhancing scattering. For piezoelectric charges, which are located in the same space as the 2DEG, it holds that $R^{\mathrm{uns}}<1$ for small q, and $R^{\mathrm{uns}}>1$ for large q. Moreover, the ratios R^{uns} for all sources in question are nearly equal to unity at small q, but appreciably greater than unity at large q. Thus, the polarization confinement effect is rather weak in forward scattering, but rather strong in backward scattering.

(iv) A comparison between the solid and dashed lines belonging to a given scattering source in Fig. 3 reveals an inequality $R^{\mathrm{scr}}<R^{\mathrm{uns}}$. This is connected with the polarization-enhanced screening. In addition, since the polarization effect on the unscreened potential is much larger than that on the screening, the ratios R^{scr} and R^{uns} exhibit similar dependencies on the in-plane wave number. For the scattering sources such as ionized dopants, surface roughness, and deformation potential, it holds that $R^{\mathrm{scr}}>1$.

It is interesting to mention that as regards the impact on the quantum confinement of the 2DEG, an increase in the electron density in the well is, according to Eq. (12), equivalent to an increase in the polarization charge density on the interface. This implies that the former can cause an enhancement not only of the screening, but also of the unscreened and screened potentials as the latter does.

(v) A comparison between the solid and dashed lines belonging to a given scattering in Fig. 4 indicates that for all mechanisms in question the mobility is reduced by polarization charges, i.e., $\mu(\sigma)<\mu^0=\mu(\sigma=0)$. The mobility reduction is due, of course, to the polarization-induced enhancement of the screened potential. The effect on surface roughness scattering is largest, while that on impurity scattering is smallest. For instance, at $x=0.25$ we have $\mu_{\mathrm{SR}}(\sigma)=3.1\times10^3$ and $\mu^0_{\mathrm{SR}}=3.7\times10^4$ cm^2/V s, while $\mu_{\mathrm{ID}}(\sigma)=2.2\times10^5$ and $\mu^0_{\mathrm{ID}}=3.3\times10^5$ cm^2/V s. At larger x, the surface roughness mobility may be degraded by up to more than one order.

It should be emphasized that the polarization-induced reduction in mobility is also established for the case of a finitely high barrier and for all scattering mechanisms under study, inclusive of alloy disorder. Thus, the overall mobility of a realistic sample is reduced. The mobility reduction was previously argued[18] merely qualitatively for surface roughness. In contrast to our conclusion, the mobility was previously argued[19] to be increased by polarization charges. The why is that this argument was based simply on the enhanced screening, ignoring totally the enhancement of the unscreened and, hence, screened scattering potentials.

It is interesting to mention that the screened potential for piezoelectric scattering is strengthened at a large in-plane wave number q, but, in difference from the other mechanisms, it is weakened at small q. However, the respective mobility is altogether found to be reduced because it is dominated by backward scattering of large q, as seen from Eq. (16).

(vi) Figure 4 also reveals that the polarization confinement may strongly modify the functional dependence of a mobility on the Al content x in addition to reducing it. Indeed, from the dashed lines, we observe that in the absence of polarization charges the functions $\mu_{\mathrm{PE}}(x)$ and $\mu_{\mathrm{DP}}(x)$ decrease, while $\mu_{\mathrm{ID}}(x)$ and $\mu_{\mathrm{SR}}(x)$ remain unchanged with a rise of x. From the solid lines, we see that in the presence of polarization charges the decrease of the mobilities becomes more rapid. In particular, instead of being a constant, $\mu_{\mathrm{SR}}(x)$ is decreasing very rapidly.

(vii) It follows from the solid lines in Fig. 4 that the mobilities limited by roughness-induced piezoelectric charges and deformation potential may be of order of or less than 10^3 cm^2/V s. Therefore, these are comparable to those limited by the so far-known scattering mechanisms. For instance, with sheet polarization charges included, at $x=0.15$ we get $\mu_{\mathrm{PE}}=1.2\times10^4$, $\mu_{\mathrm{DP}}=2.1\times10^4$ cm^2/V s, at $x=0.25$: $\mu_{\mathrm{PE}}=4.1\times10^3$, $\mu_{\mathrm{DP}}=6.2\times10^3$ cm^2/V s, and at $x>0.55$: $\mu_{\mathrm{PE}}\approx\mu_{\mathrm{DP}}\approx\mu_{\mathrm{SR}}<1\times10^3$ cm^2/V s. Meanwhile, the impurity scattering is of minor importance for all x ($\mu_{\mathrm{ID}}\approx2\times10^5$ cm^2/V s).

C. Comparison with experiment

In what follows, we are dealing with the recent experimental data[12,19] about the carrier density dependence of the 2DEG mobility in single and double AlGaN/GaN heterostructures at high densities ($\gtrsim5\times10^{12}$ cm^{-2}). For quantitative explanation, we have calculated this functional dependence for the realistic samples, taking into account the effects from both the finiteness of the potential barrier height and the polarization confinement.

We are first concerned with the AlGaN/GaN SH sample studied in Ref. 12 as described above, but now with a fixed Al content $x=0.25$, so a lattice mismatch $\epsilon_{\parallel}=0.61\%$. The barrier height is assumed to be $V_0=0.4$ eV. The partial and overall 2DEG mobilities are plotted versus electron density n_{s} in Fig. 5, where the 25 K experimental data[12] is also reproduced for a comparison.

Next, the 2DEG mobilities of interest are plotted versus electron density n_{s} for an SH and a DH sample of an Al content $x=0.15$ in Fig. 6, where the 4.2 K experimental data reported in Ref. 19 are also presented. The SH sample consists of AlGaN (300 Å)/GaN (1 μm), and the DH of AlGaN (300 Å)/GaN (200 Å)/AlGaN (1000 Å). The AlGaN (300 Å) barrier is doped with a Si donor density $N_{\mathrm{I}}=5\times10^{18}$ cm^{-3}. This doped layer in both samples is nominally accompanied by no spacer. However, as indicated before, because of Coulomb repulsions from positive sheet polarization charges on the interface there must be a spacer of the minimal thickness $L_{\mathrm{s}}=L_\sigma\sim6$ Å. The barrier height is assumed to be $V_0=0.7$ eV.

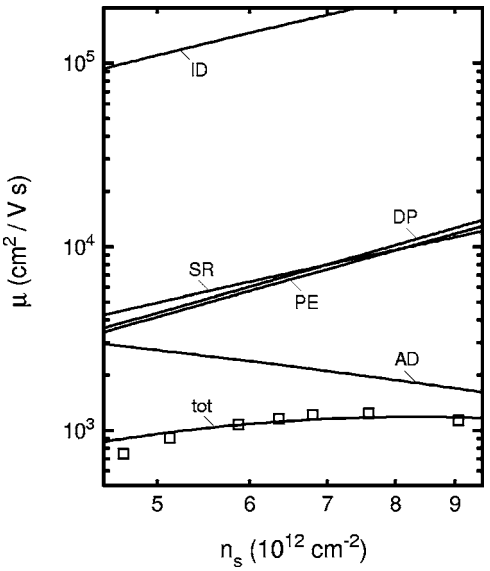

FIG. 5. Different 2DEG mobilities of an AlGaN/GaN SH sample of a finitely high potential barrier and an Al content $x=0.25$ vs sheet electron density n_s. The interpretation is the same as in Fig. 4. The 25 K experimental data reported in Ref. 12 are marked by squares.

The lattice mismatch in the above systems is defined by Eq. (2). The in-plane lattice constants at the surface-side interface may be crudely estimated as follows. The two layers around a given interface are assumed[68,69] to share the same in-plane lattice constant whose value is fixed so as to minimize the elastic free energy. As a result, the lattice mismatch in the SH sample in question is equal to $\epsilon_{\|}=0.36\%$, while that in the DH is smaller, $\epsilon_{\|}\sim 0.14\%$.

It was experimentally shown[70,71] that the interface of a heterostructure becomes smoother with a decrease of the lattice mismatch. Accordingly, the interface profile for the SH sample is chosen with an amplitude $\Delta=2$ Å and a correlation length $\Lambda=82$ Å, while that for the DH with $\Delta=1.5$ Å and $\Lambda=82$ Å. This is in agreement with an observation[19] that the interface morphology is improved in the DH sample.

In Figs. 5 and 6, the contributions from phonon and dipole scatterings to the overall mobility are neglected, since the respective partial mobilities are found[18,24] to be $\gtrsim 2\times 10^5$ cm^2/V s, thus being much larger than the measured ones. From the lines obtained in Figs. 5 and 6, we may draw the following conclusions.

(i) As can be observed from Fig. 5, the overall mobility $\mu_{\rm tot}(n_s)$ calculated for the SH sample studied in Ref. 12 well reproduces the 2DEG mobility measured at the carrier densities in use. This exhibits a nonmonotonic function of the electron density with a pronounced maximum at $n_s\approx 8\times 10^{12}$ cm^{-2}. Meanwhile, the calculated partial mobilities are monotonic functions. Thus, the peak of the overall mobility must arise as a result of competition between increasing and decreasing trends. Indeed, the functions $\mu_{\rm ID}(n_s)$, $\mu_{\rm SR}(n_s)$, $\mu_{\rm PE}(n_s)$, and $\mu_{\rm DP}(n_s)$ are found to increase with a rise of n_s, whereas $\mu_{\rm AD}(n_s)$ to decrease, altogether producing the overall-mobility peak.

It is worthy to recall that in order to explain their experimental data about the 2DEG mobility reported in Ref. 12, the authors had to invoke the unclear concept of interface charges. Moreover, they had to assume a simplistic interface profile with a very short correlation length (δ-correlated interface), neglecting its spectral distribution, which is very suspect.[22] Hence, their $\mu_{\rm SR}(n_s)$ is a decreasing function of the electron density, which is opposite to ours.

(ii) Figure 5 also indicates that the functions $\mu_{\rm PE}(n_s)$ and $\mu_{\rm DP}(n_s)$ are nearly equal to $\mu_{\rm SR}(n_s)$ in the used region of n_s, but much smaller than $\mu_{\rm ID}(n_s)$ (about twenty times). This means that in the SH sample studied in Ref. 12, the scatterings by roughness-induced piezoelectric charges and deformation potential are so important as by surface roughness (and alloy disorder), while ionized dopants are much less relevant.

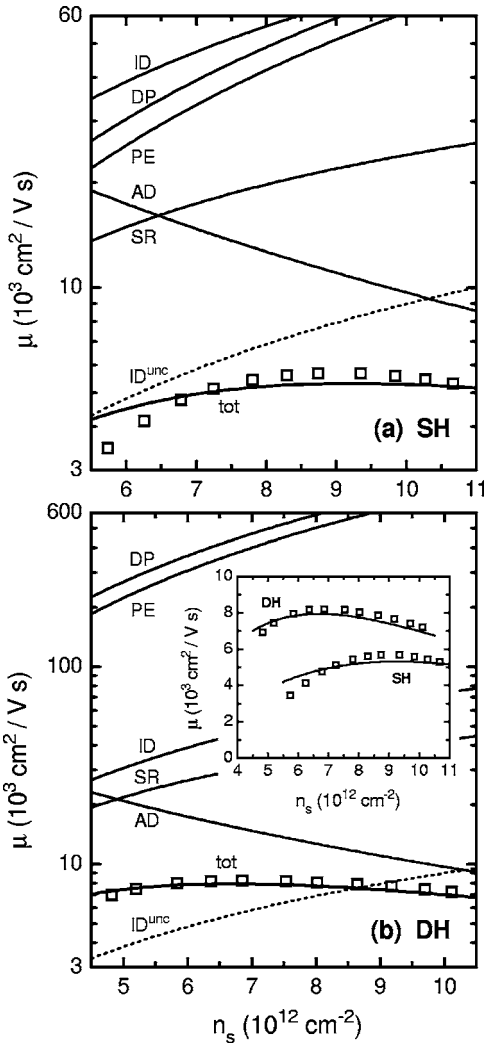

FIG. 6. Different 2DEG mobilities of (a) an AlGaN/GaN SH and (b) an AlGaN/GaN/AlGaN DH sample of a finitely high potential barrier and an Al content $x=0.15$ vs sheet electron density n_s. The interpretation is the same as in Fig. 4, and the dotted line refers to the impurity-limited mobility without ionic correlation and minimal spacer $\mu_{\rm ID}^{\rm unc}$. The 4.2 K experimental data reported in Ref. 19 are marked by squares. The inset shows the overall and measured mobilities for both the SH and DH samples in nonlogarithmic ordinate axis scale.

(iii) It is clearly seen from Fig. 6 that the overall mobilities $\mu_{tot}(n_s)$ calculated for the SH and DH samples studied in Ref. 19 almost coincide with the measured carrier density dependencies, showing the enhanced mobility in the DH [see the inset in Fig. 6(b)].

In the SH sample [Fig. 6(a)], the increasing trend of the overall mobility is due to the mobilities limited by surface roughness, piezoelectric charges, deformation potential, and ionized dopants. Compared to the SH sample, the lattice mismatch in the DH [Fig. 6(b)] is smaller, so that its partial mobilities $\mu_{PE}(n_s)$ and $\mu_{DP}(n_s)$ are larger (about five times). Therefore, piezoelectric charges and deformation potential in the DH are of minor importance, and the increasing trend of its overall mobility is due to the mobilities limited only by surface roughness and ionized dopants, hence its peak must be raised and shifted toward lower electron densities.

It is worthy to recall that the experimental data for the SH and DH samples in Fig. 6 was reported in Ref. 19 with no quantitative description. In addition, the enhanced mobility in the DH sample was qualitatively treated and was ascribed to the enhancement of the polarization confinement owing to negative sheet piezoelectric charges on its substrate-side interface.[72] However, as indicated above, the polarization confinement gives rise to a decrease of the mobility rather than its increase.

(iv) Finally, Fig. 6 also shows that when neglecting the effects due to the ionic correlation and minimal spacer, impurity scattering is drastically enhanced. Therefore, the respective mobility is found to be reduced by about one order, so that it becomes smaller than that measured $\mu_{ID}^{unc} < \mu_{expt}$ for the SH sample at $n_s \lesssim 5.5 \times 10^{12}$ cm^{-2}, and for the DH at $n_s \lesssim 8.5 \times 10^{12}$ cm^{-2}. This unreasonable result implies that these effects are important in explaining high values of the 2DEG mobility observed at high doping levels.

VI. SUMMARY

In this paper we have presented a comprehensive treatment of the low-temperature mobility of the 2DEG in wurtzite group-III-nitride heterostructures, e.g., AlGaN/GaN SH and DH samples. In distinction from the existing theories, we have derived simple analytic expressions, which explicitly describe the influence arising from sheet (piezoelectric and spontaneous) polarization-induced charges on the electron envelope wave function and, hence, on the scattering rates for different scattering processes limiting the 2DEG mobility.

We have proved that the effects due to the polarization confinement are counteracting. On one hand, this enhances the screening, so reducing the scattering and increasing the mobility. On the other hand, this generally enhances the unscreened potentials for the scattering processes under study, so reducing the mobility. Altogether, their screened potentials are enhanced. Opposite to the earlier theory,[19] the electron mobility may be remarkably reduced by the polarization confinement. The sheet polarization charges can cause a drastic enhancement of the screening in two ways, viz., by elevating the number of 2D electrons involved in the screening effect, as already known, and also by elevating the efficiency of their screening act.

We have introduced the roughness-induced scatterings, viz., by piezoelectric charges and deformation potential, into the 2DEG transport theory for wurtzite III-nitride heterostructures as new mechanisms. Despite being located in the GaN well, the mechanisms depend not only on the interface profile but also the lattice mismatch, i.e., the residual strain in the AlGaN barrier. These are found to be among the key scattering sources that dominates the mobility, and these become more important when increasing the alloy content.

We have succeeded in handling some challenging problems in the theory of the low-temperature 2DEG mobility in wurtzite III-nitride heterostructures. We have been able to provide a good quantitative explanation of the recent experimental data about the high-density mobility in AlGaN/GaN SH and DH samples, e.g., its nonmonotonic dependence on the carrier density and its enhancement in the DH sample, which could not be understood if based merely on the conventional sources.

[1] S. Nakamura, T. Mukai, and M. Senoh, Appl. Phys. Lett. **64**, 1687 (1994).
[2] A. Ozgur, W. Kim, A. Botchkarev, A. Salvador, S. N. Mohamad, B. Sverdlov, and H. Morkoç, Electron. Lett. **31**, 1389 (1995).
[3] Y. F. Wu, B. P. Keller, S. Keller, D. Dapolnek, P. Kozodoy, S. P. Denbaars, and U. K. Mishra, Appl. Phys. Lett. **69**, 1438 (1996).
[4] S. C. Binari, J. M. Redwing, G. Kelner, and W. Kruppa, Electron. Lett. **33**, 242 (1997).
[5] R. Gaska, Q. Chen, J. Yang, A. Osinsky, M. A. Khan, and M. S. Shur, IEEE Electron Device Lett. **18**, 492 (1997).
[6] O. Ambacher, J. Phys. D **31**, 2653 (1998).
[7] J. M. Redwing, M. A. Tischler, J. S. Flynn, S. Elhamri, M. Ahoujja, R. S. Newrock, and W. C. Mitchel, Appl. Phys. Lett. **69**, 963 (1996).
[8] R. Gaska, Y. W. Yang, A. Osinsky, Q. Chen, M. A. Khan, A. O. Orlov, G. L. Snider, and M. S. Shur, Appl. Phys. Lett. **72**, 707 (1998).
[9] R. Gaska, M. S. Shur, A. D. Bykhovski, A. O. Orlov, and G. L. Snider, Appl. Phys. Lett. **74**, 287 (1999).
[10] I. P. Smorchkova, C. R. Elsass, J. P. Ibbetson, R. Vetury, B. Heying, P. Fini, E. Haus, S. DenBaars, J. S. Spect, and U. K. Mishra, J. Appl. Phys. **86**, 4520 (1999).
[11] Y. Zhang, I. P. Smorchkova, C. R. Elsass, S. Keller, J. P. Ibbetson, S. Denbaars, U. K. Mishra, and S. Singh, J. Appl. Phys. **87**, 7981 (2000).
[12] J. Antoszewski, M. Gracey, J. M. Dell, L. Faraone, T. A. Fisher, G. Paris, Y.-F. Wu, and U. K. Mishra, J. Appl. Phys. **87**, 3900 (2000).
[13] Z. W. Zheng, B. Shen, Y. S. Gui, C. P. Jiang, N. Tang, R. Zhang, Y. Shi, Y. D. Zheng, S. L. Guo, G. Z. Zheng, J. H. Chu, T. Someya, and Y. Arakawa, Appl. Phys. Lett. **82**, 1872 (2003).
[14] L. Hsu and W. Walukiewicz, Phys. Rev. B **56**, 1520 (1997); Appl.

Phys. Lett. **73**, 339 (1998).
[15] R. Oberhuber, G. Zandler, and P. Vogl, Appl. Phys. Lett. **73**, 818 (1998).
[16] T. Li, R. P. Joshi, and C. Fazi, J. Appl. Phys. **88**, 829 (2000).
[17] L. Hsu and W. Walukiewicz, J. Appl. Phys. **89**, 1783 (2001).
[18] T.-H. Yu and K. F. Brennan, J. Appl. Phys. **89**, 3827 (2001).
[19] N. Maeda, T. Saitoh, K. Tsubaki, T. Nishida, and N. Kobayashi, Appl. Phys. Lett. **76**, 3118 (2000).
[20] M. J. Manfra, L. N. Pfeiffer, K. W. West, H. L. Stormer, B. W. Baldwin, J. W. P. Hsu, D. V. Lang, and R. J. Molnar, Appl. Phys. Lett. **77**, 2888 (2000).
[21] J. R. Juang, T.-Y. Huang, T.-M. Chen, M.-G. Lin, G.-H. Kim, Y. Lee, C.-T. Liang, D. R. Hang, Y. F. Chen, and J.-I. Chyi, J. Appl. Phys. **94**, 3181 (2003).
[22] F. Schäffler, Semicond. Sci. Technol. **12**, 1515 (1997).
[23] R. J. P. Lander, M. J. Kearney, A. I. Horrell, E. H. C. Parker, P. J. Phillips, and T. E. Whall, Semicond. Sci. Technol. **12**, 1604 (1997).
[24] D. Jena, A. C. Gossard, and U. K. Mishra, J. Appl. Phys. **88**, 4734 (2000).
[25] A. Bykhovski, G. Gelmont, and M. Shur, J. Appl. Phys. **74**, 6734 (1993).
[26] F. Bernardini, V. Fiorentini, and D. Vanderbilt, Phys. Rev. B **56**, R10024 (1997).
[27] N. Maeda, T. Nishida, N. Kobayashi, and M. Tomizawa, Appl. Phys. Lett. **73**, 1856 (1998).
[28] Y. Zhang and J. Singh, J. Appl. Phys. **85**, 587 (1999).
[29] M. S. Shur, A. D. Bykhovski, and R. Gaska, Solid-State Electron. **44**, 205 (2000).
[30] R. M. Feenstra and M. A. Lutz, J. Appl. Phys. **78**, 6091 (1995).
[31] D. N. Quang, V. N. Tuoc, N. H. Tung, and T. D. Huan, Phys. Rev. Lett. **89**, 077601 (2002); Phys. Rev. B **68**, 153306 (2003).
[32] D. N. Quang, V. N. Tuoc, and T. D. Huan, Phys. Rev. B **68**, 195316 (2003).
[33] D. N. Quang, V. N. Tuoc, T. D. Huan, and P. N. Phong, Phys. Rev. B **70**, 195336 (2004).
[34] D. N. Quang, N. H. Tung, V. N. Tuoc, N. V. Minh, and P. N. Phong, Phys. Rev. B **72**, 115337 (2005).
[35] O. Ambacher, B. Foutz, J. Smart, J. R. Shealy, N. G. Weimann, K. Chu, M. Murphy, A. J. Sierakowski, W. J. Shaff, L. F. Eastman, R. Dimitrov, A. Mitchell, and M. Stutzmann, J. Appl. Phys. **87**, 334 (2000).
[36] T. Ando, A. B. Fowler, and F. Stern, Rev. Mod. Phys. **54**, 437 (1982).
[37] M. Morkoç, F. Hamdani, and A. Salvador, in *Gallium Nitride (GaN) I*, Vol. 50 of Semiconductors and Semimetals, edited by J. I. Pankove and T. D. Moustakas (Academic, San Diego, 1998), p. 193.
[38] T. Ando, J. Phys. Soc. Jpn. **51**, 3893 (1982); **51**, 3900 (1982).
[39] G. Bastard, *Wave Mechanics Applied to Semiconductor Heterostructures* (Les Editions de Physique, Paris, 1988).
[40] Y. Okuyama and N. Tokuda, Phys. Rev. B **40**, 9744 (1989).
[41] M. Suzuki, T. Uenoyama, and A. Yanase, Phys. Rev. B **52**, 8132 (1995).
[42] L. W. Wong, S. J. Cai, R. Li, K. Wang, H. W. Jiang, and M. Chen, Appl. Phys. Lett. **73**, 1391 (1998).
[43] P. M. Asbeck, E. T. Yu, S. S. Lau, G. J. Sullivan, J. Van Hove, and J. Redwing, Electron. Lett. **33**, 1230 (1997).
[44] A. Gold and W. Götze, J. Phys. C **14**, 4049 (1981); Phys. Rev. B **33**, 2495 (1986).
[45] M. J. Kearney and A. I. Horrell, Semicond. Sci. Technol. **14**, 211 (1999).
[46] F. Stern and W. E. Howard, Phys. Rev. **163**, 816 (1967).
[47] A. Gold, Phys. Rev. B **35**, 723 (1987).
[48] M. Jonson, J. Phys. C **9**, 3055 (1976).
[49] E. F. Schubert, J. M. Kuo, R. F. Kopf, H. S. Luftman, L. C. Hopkins, and N. J. Sauer, J. Appl. Phys. **67**, 1969 (1990).
[50] A. L. Efros, F. G. Pikus, and G. G. Samsonidze, Phys. Rev. B **41**, 8295 (1990).
[51] D. N. Quang, N. N. Dat, and D. V. An, Phys. Lett. A **182**, 125 (1993).
[52] D. N. Quang and N. H. Tung, Phys. Status Solidi B **207**, 111 (1998).
[53] A. Asgari, M. Kalafi, and L. Faraone, J. Appl. Phys. **95**, 1185 (2004).
[54] R. Enderlein and N. J. M. Horing, *Fundamentals of Semiconductor Physics and Devices* (World Scientific, Singapore, 1997).
[55] S. Chichibu,, A. Shikanai, T. Azuhata, T. Sota, A. Kuramata, K. Horino, and S. Nakamura, Appl. Phys. Lett. **68**, 3766 (1996).
[56] A. Shikanai, T. Azuhata, T. Sota, S. Chichibu, A. Kuramata, K. Horino, and S. Nakamura, J. Appl. Phys. **81**, 417 (1997).
[57] K. Kim, W. R. L. Lambrecht, and B. Segall, Phys. Rev. B **53**, 16 310 (1996).
[58] G. Martin, S. Strite, A. Botchkarev, A. Agarwal, A. Rockett, H. Morkoç, W. R. L. Lambrecht, and B. Segall, Appl. Phys. Lett. **65**, 610 (1994).
[59] G. Martin, A. Botchkarev, A. Rockett, and H. Morkoç, Appl. Phys. Lett. **68**, 2541 (1996).
[60] A. D. Bykhovski, R. Gaska, and M. S. Shur Appl. Phys. Lett. **73**, 3577 (1998).
[61] W. Shan, R. J. Hauenstein, A. J. Fischer, J. J. Song, W. G. Perry, M. D. Bremser, R. F. Davis, and B. Goldenberg, Phys. Rev. B **54**, 13460 (1996).
[62] M. Suzuki and T. Uenoyama, J. Appl. Phys. **80**, 6868 (1996).
[63] S. L. Chuang and C. S. Chang, Semicond. Sci. Technol. **12**, 252 (1997).
[64] K. Shimada, T. Sota, and K. Suzuki, J. Appl. Phys. **84**, 4951 (1998).
[65] M. Kumagai, S. L. Chuang, and H. Ando, Phys. Rev. B **57**, 15303 (1998).
[66] S. H. Park and S. L. Chuang, J. Appl. Phys. **87**, 353 (2000).
[67] R. M. Feenstra, M. A. Lutz, F. Stern, K. Ismail, P. M. Mooney, F. K. LeGoues, C. Stanis, J. O. Chu, and B. S. Meyerson, J. Vac. Sci. Technol. B **13**, 1608 (1995).
[68] E. Anastassakis, Solid State Commun. **78**, 347 (1991).
[69] B. Jogai, J. Appl. Phys. **91**, 3721 (2002).
[70] Y. H. Xie, G. H. Gilmer, C. Roland, P. J. Silverman, S. K. Buratto, J. Y. Cheng, E. A. Fitzgerald, A. R. Kortan, S. Schuppler, M. A. Marcus, and P. H. Citrin, Phys. Rev. Lett. **73**, 3006 (1994).
[71] S. Arulkumaran, T. Egawa, H. Ishikawa, and T. Jimbo, J. Vac. Sci. Technol. B **21**, 888 (2003).
[72] N. Maeda, T. Saitoh, K. Tsubaki, T. Nishida, and N. Kobayashi, Phys. Status Solidi B **216**, 727 (1999).